Journal of Alloys and Compounds 794 (2019) 21–25

Contents lists available at ScienceDirect

Journal of Alloys and Compounds

journal homepage: http://www.elsevier.com/locate/jalcom

Growth and optical properties of $LiTm(WO_4)_2$ crystal

K. Kokh [a, b, *], A. Kraghzda [a, b], V. Svetlichnyi [c], E. Galashov [b], S. Rashchenko [a, b], Yu. Seryotkin [a, b], A. Kuznetsov [a, b], A. Maillard [d], B. Uralbekov [e], A. Kokh [a]

[a] Sobolev Institute of Geology and Mineralogy, Novosibirsk, Russia
[b] Novosibirsk State University, Russia
[c] Siberian Physical–Technical Institute of Tomsk State University, Tomsk 634050, Russia
[d] Lorraine University and Supelec, Metz 57070, France
[e] Center of Physical-Chemical Methods of Research and Analysis, Al-Farabi Kazakh National University, Almaty 050000, Kazakhstan

ARTICLE INFO

Article history:
Received 1 June 2017
Received in revised form
10 April 2019
Accepted 12 April 2019
Available online 25 April 2019

Keywords:
Double tungstates
Thulium
Crystal growth
Structure
Optical properties

ABSTRACT

The bulk crystals of $LiTm(WO_4)_2$ with dimensions up to $10 \times 15 \times 3$ mm have been obtained for the first time. Crystals of the compound melts congruently at 1007 °C, however melt crystallization of high quality crystal is impossible due to phase transition at ~920 °C. The top seeded solution method from Li_2WO_4-WO_3 flux was successfully applied reducing the growth temperature below 900 °C. According to single crystal x-ray measurements, the crystal corresponds to the $P2/n$ space group. Raman, luminescence and transmission spectra reveal optical features owing to the presence of thulium ions, and therefore the materials could be further studied in the scope of laser and luminescence applications.

1. Introduction

Much attention has been given in recent years to the study of tungstates, especially those containing rare earth elements. Crystal tungstates were shown to be promising for a variety of laser [1,2], scintillator [3] and phosphor [4,5] applications. Single crystals of double tungstates of rare-earth and alkali elements are of special interest in laser industry. In potassium-containing matrices, for example, the active dopant concentration may be quite high without substantial fluorescence quenching because the inter-ion distance is large. For instance, Yb-doped potassium-yttrium (KYW) and -gadolinium (KGW) crystals are the main compact media to generate ~1 μm fs pulses [6]. Another promising host of Yb and Tm active ions is K-Lu double tungstate (KLuW) [7]. These KYW, KGW and KLuW materials crystallize in $KY(WO_4)_2$ structural type (space group $C2/c$). In contrast, sodium based rare earth tungstates which may also effectively host Yb, crystallize in scheelite structural type (space group $I4_1/a$) with disordered mono- and trivalent cations. The latter results in broadened absorption and fluorescence bandwidth [8]. The compounds like $NaY(WO_4)_2$ and $NaGd(WO_4)_2$ melt congruently, and thus may be grown to large crystal sizes by the Czochralski method [9].

Lithium has the smallest radius in the alkali metal series, which results in further structural changes for lithium-based double tungstates. According to the review of Klevtsov and Klevtsova [10], the scheelite-type $I4_1/a$ structure is stable only as a high-temperature α-modification of all $LiLn(WO_4)_2$ compounds. At intermediate temperatures, monoclinic β-modification (space group $P2/n$) becomes stable for Ln = Tb…Lu. At low temperature, compounds with Ln = Eu…Lu crystallize in monoclinic γ-modification (space group $P2/c$), whereas those with Ln = La…Sm adopt the triclinic $P\bar{1}$ structure [11]. Both monoclinic β and γ modifications are closely related to wolframite structure based on the zigzag chains of edge-shared octahedra. In the β modification there are two types of these chains: one built from WO_6 octahedra, and the other from alternating LiO_6 and LnO_6 octahedra. In contrast, in the low-temperature γ modification all cations form separate chains. The β modification ($P2/n$) is often referred as 'LiYb$(WO_4)_2$ structural type'; the γ modification ($P2/c$) corresponds to the $NaIn(WO_4)_2$ structural type. We should also note a potentially confusing observation that both β and γ modifications have the same space group, namely $P2/c$ (#13), but non-conventional setting $P2/n$ is used in the case of β modification to obtain a more orthogonal unit cell.

Use of the rare earth element thulium (Tm) can improve the

* Corresponding author. IGM SB RAS, Koptyuga ave., 3, Novosibirsk 630090, Russia.
E-mail address: kokh@igm.nsc.ru (K. Kokh).

https://doi.org/10.1016/j.jallcom.2019.04.133
0925-8388/

operation of functional materials. Thulium can be substituted for unstable europium ion (Eu^{2+}) and provides an excellent luminescent activator in the blue spectral range due to $^1D_2 \rightarrow {}^3F_4$ transition at ~450 nm [12]. Blue phosphorescence can be modified with elements that emit red and green wavelengths and provides white light from UV LED chip [13,14]. The electron transition $^3F_4 \rightarrow {}^3H_6$ in Tm is used for laser generation in the two-micron range [15]. This wavelength is much safer for eyes than that below 1.5 μm and may be used to improve laser safety in many applications such as lidar, surgery and air data transferring. Finally, Tm excitation is typically produced at 700–1100 nm with commercial InGaAs and AlGaAs diodes.

Use of tiny diodes sources can pave the way to compact chip lasers. Recently a highly efficient waveguide Tm-laser was demonstrated [16] where the active layer was grown on undoped substrate using a high temperature solution liquid phase epitaxy.

Crystals of the Li*Ln*$(WO_4)_2$ family have been previously synthesized and characterized for laser applications [17–21]. However, no data exist on the LiTm tungstate except the early X-ray powder data [10,22,23]. In this work, we describe conditions needed to grow crystals of $LiTm(WO_4)_2$ (LTW) and report its structural and optical properties. The obtained results on high Tm concentration compound LTW could be interesting for both phosphor and laser applications.

2. Experimental

Dehydrated $Tm(NO_3)_3$ (99.99%), WO_3 (99.99%), and Li_2CO_3 (99.999%) were used as starting reagents for the synthesis by solid-state reaction. After weighing out according to proportion $0{,}5\ Tm(NO_3)_3 + 0{,}5\ Li_2CO_3 + 2WO_3$, the mixture was heated in air at 550 °C in a platinum crucible and kept at this temperature for 1 day.

Single crystal growth using Li_2WO_4-WO_3 flux was carried out by the top seeded solution method. A platinum crucible with a diameter of 60 mm and 80 mm of height was used, and the crucible was covered with a cap to decrease volatilization of the components. Crystal growth was encouraged by controlling the cooling rate and seed rotating speed at 0.5–0.7 deg/day and 1.2–2 rpm, respectively. After 2–4 weeks of growth, the crystal was cooled at a rate of 15 deg/hour. Thermal properties under N_2 gas flow were investigated by differential thermal analysis (DTA) using a NETZSCH STA 449F3 thermal analyzer. The heating/cooling rate was 15 °C/min.

A single-crystal X-ray diffraction experiment was performed at STOE IPDS-2T diffractometer equipped with a Mo source (graphite monochromator) and IP detector. The collected data were handled in CrysAlisPro software using ESPERANTO protocol [24]. The SHELX-2014 software [25] in WinGX suite [26] was used for structure solution and refinement. The powder polycrystalline sample was studied on the ARL X'TRA Bragg-Brentano diffractometer using CuKα radiation. The diffraction data were analyzed by the Rietveld method using GSAS-II software [27].

Vis- and IR absorption spectra of the sample were recorded using a Cary 100 spectrometer, Varian (operation range 200–900 nm, spectral resolution of 1 nm) and a FTIR spectrometer Tenzor 27, Bruker (375-7000 cm^{-1}, spectral resolution 4 cm^{-1}). Fluorescence was recorded by CM2203, SOLAR. Raman spectra were analyzed using a Renishaw InVia spectrometer with excitation sources at 532 and 785 nm. All optical measurements were carried out at room temperature and with unpolarized light.

3. Result and discussion

A review of previously published data [28] indicates that $LiTm(WO_4)_2$ melts at 1007°C and demonstrates polymorphic transitions α-$I4_1/a$ → β-$P2/n$ → γ-$P2/c$ at 976°C and 840°C, respectively. However, the powder diffraction pattern of the sample synthesized at 500°C (Fig. 1a) belongs to the β-modification of

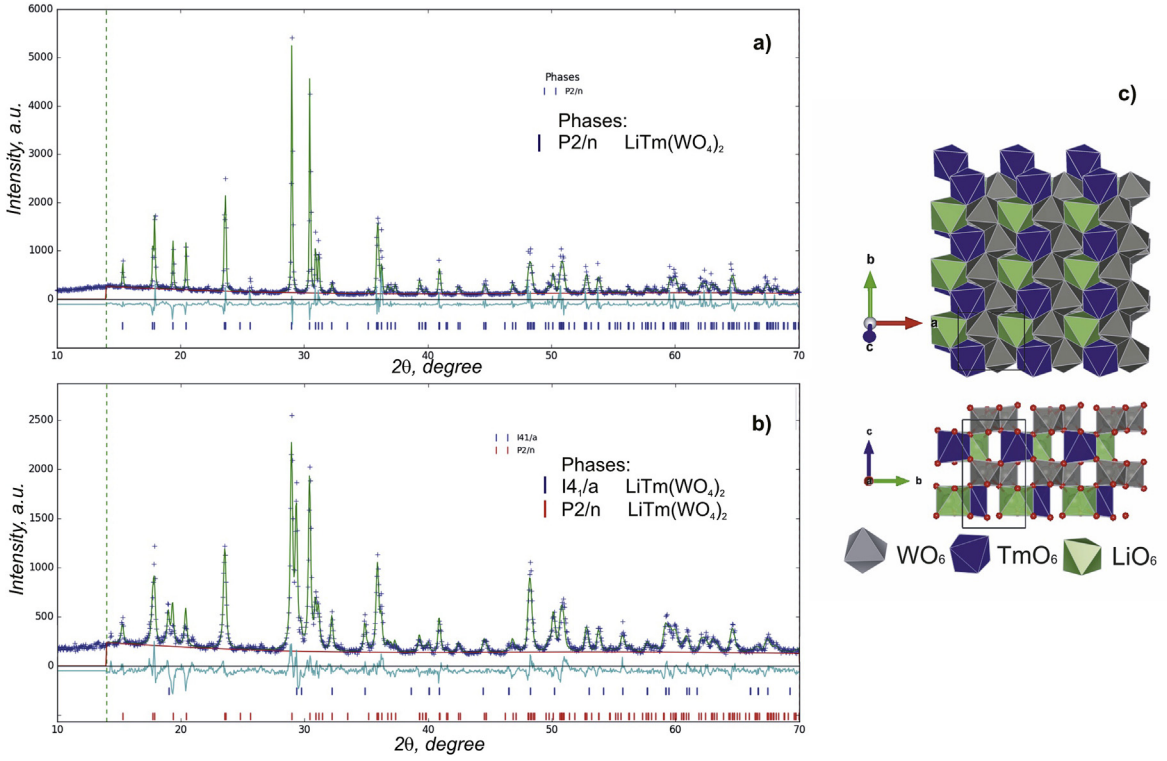

Fig. 1. XRD patterns and results of Rietveld analysis for $LiTm(WO_4)_2$ sample (a) Synthesized at 500 °C; (b) Quenched from 1100 °C. Experimental pattern is shown in blue, calculated pattern – in green, and difference curve – in cyan. Strokes mark positions of reflections. (c) Crystal structure of $LiTm(WO_4)_2$. (For interpretation of the references to colour in this figure legend, the reader is referred to the Web version of this article.)

$LiTm(WO_4)_2$, which was confirmed by Rietveld refinement on the basis of the structural model obtained from a single-crystal diffraction experiment (see below). Thermal analysis of the sample showed one endothermic effect of melting at 1007°C upon heating, and two exo-peaks at 1000 °C and 920°C upon cooling (Fig. 2).

In order to assess the potential for incongruent melting of LTW, the sample was heated to 1100 °C and then rapidly cooled to room temperature. The Rietveld analysis revealed that the quenched sample represents a mixture of tetragonal α and monoclinic β modifications in proportion 1:3 (Fig. 1b). Herewith, the compound most likely melts congruently and the second peak at the cooling stage corresponds to the structural transformation from tetragonal to monoclinic β phase. Thus, it is necessary to use a melt-solution to lower the crystallization process below the phase transition temperature.

Solubility of LTW was studied in Li_2WO_4-WO_3 flux, using a modified visual polythermic technique [29]. The flux was chosen as eutectic composition $0.45Li_2WO_4+0.55WO_3$ with the melting temperature of 744°C. Results show that LTW has a wide region of primary crystallization in the flux (Fig. 3). The flux could be also favorable for the growth of other tungstate crystals.

The first growth run, using a platinum wire, resulted in a druse with plate-like grains about 0.5 mm thick (Fig. 4a). Because of intensive evaporation all the experiments were conducted at LTW concentration <30% by weight. The plates were then used for a seeded growth experiment but no monocrystal was obtained. All experiments led to a polycrystalline aggregate of parallel plates. This phenomenon may be the result of crystal splitting due to obstruction of crystallization front by flux components. The size of the plates was sufficiently increased by applying seed rotation during growth. As a result, transparent grains with the dimensions up to 10 × 15 × 3 mm were obtained (Fig. 4c).

Single-crystal X-ray diffraction was performed on a high quality single crystal of 0.04 × 0.06 × 0.19 mm^3 selected under a polarizing microscope. The details of data collection and structure refinement are summarized in Table 1. All structural data are listed in Table 2. Table 3 summarizes the interatomic distances. Note that we used the recommended non-conventional *P*2/*n* setting for the *P*2/*c* space group to avoid too oblique *β* angle.

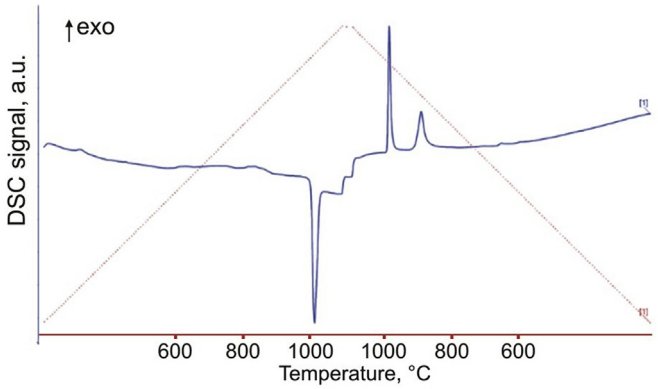

Fig. 2. DSC curve of synthesized $LiTm(WO_4)_2$.

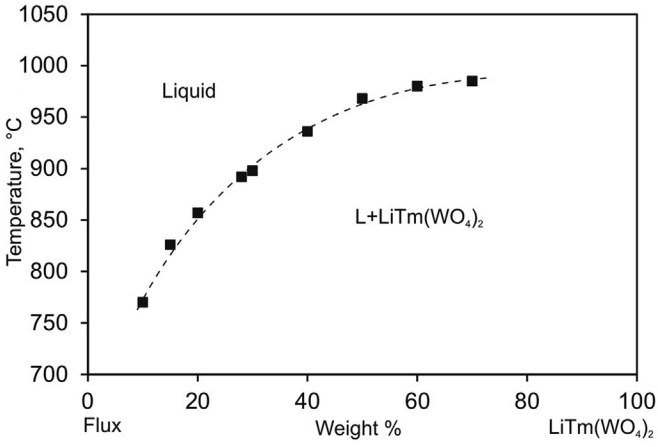

Fig. 3. Solubility curve of $LiTm(WO_4)_2$ in $0.45Li_2WO_4+0.55WO_3$ flux.

Table 1
Parameters of single-crystal data collection and structure refinement.

Formula	$LiTm(WO_4)_2$	
Formula weight	671.57	
Space group	P 2/n (No. 13)	P 2/c (No.13)[a]
a(Å)	4.99159(1)	9.9207(2)
b(Å)	5.78366(1)	5.7837(1)
c (Å)	9.92072(2)	10.8124(2)
B (°)	93.72180(2)	152.569(6)
V ($Å^3$)	285.806(10)	285.806(10)
Calculated density (g/cm^3)	7.804	
Absorption coefficient (mm^{-1})	55.536	
F(000)	568	
θ range (°)	2.0571–29.5565	
hkl limits	$-6<h<6$, $-8<k<8$, $-13<l<13$	
Measured reflections	8229	
Unique reflections	796	
Reflection with $I>2\delta(I)$	783	
R_{int}	0.0833	
Refined parameters	54	
R factor ($I>2\delta(I)$)	$R1=0.0354$ $wR2=0.1046$	
R factor (all data)	$R1=0.0360$ $wR2=0.1054$	
Residual electron density($e/Å^3$)	Max = 5.942 min −3.951 av = 0.763	

[a] Parameters for *P*2/*c* structure are presented for comparison.

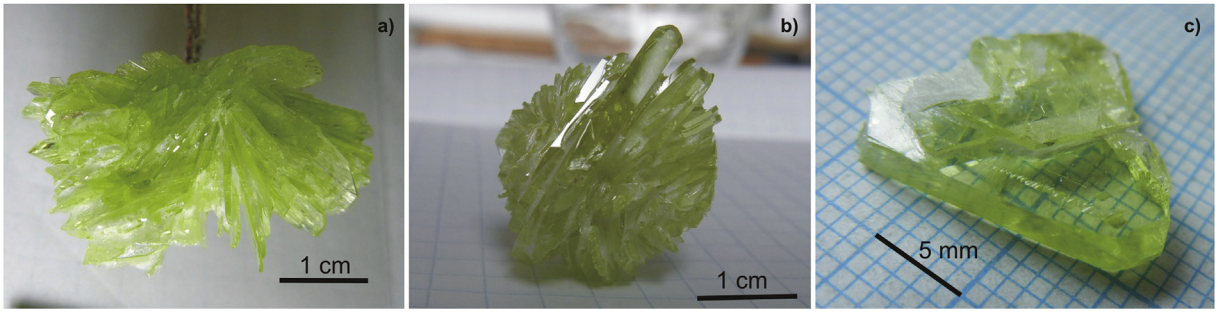

Fig. 4. $LiTm(WO_4)_2$ crystals: (a) spontaneously grown druse; (b) aggregate of parallel plates grown on seed; (c) transparent grain.

Table 2
Positional parameters of $LiTm(WO_4)_2$ structure.

Atom	Wyckoff	x	y	z	Ueq
Li	2f	0.250000	−0.774(6)	−0.250000	0.021(6)
Tm	2e	0.250000	0.19809(9)	−0.750000	0.0095(2)
W	4g	0.224876(6)	−0.31831(6)	−0.51622(4)	0.0071(2)
O1	4g	0.093(12)	−0.1237(11)	−0.6353(6)	0.008(1)
O2	4g	0.3939(12)	−0.125(1)	−0.3901(6)	0.010(1)
O3	4g	0.4675(12)	−0.5861(11)	−0.3867(6)	0.011(1)
O4	4g	0.0513(12)	−0.6077(12)	−0.5961(6)	0.0095(11)

Atom	U_{11}	U_{22}	U_{33}	U_{23}	U_{13}	U_{12}
Tm	0.0125(3)	0.0093(3)	0.0070(3)	0	0.0023(2)	0
W	0.0066(2)	0.0077(3)	0.0071(3)	0.00064(1)	0.0008(1)	0.00024(8)
O1	0.011(3)	0.004(3)	0.010(3)	0.002(2)	−0.002(2)	−0.002(2)
O2	0.01(3)	0.010(3)	0.010(3)	−0.002(2)	0.001(2)	−0.002(2)
O3	0.011(2)	0.009(3)	0.013(2)	0.0014(2)	0.002(2)	0.004(2)
O4	0.011(2)	0.007(3)	0.011(3)	0.002(2)	0.003(2)	−0.001(2)

Table 3
Principal interatomic distances.

Atoms	Distance/Å
Li-O_1 (×2)	2.079(11)
Li-O_2 (×2)	2.59(2)
Li-O_3 (×2)	2.10(2)
Li-O Av.	2.25
W-O_1	1.774(6)
W-O_2	1.795(6)
W-O_3	1.848(6)
W-O_4	1.971(6)
W-O_4(×1)	2.073(6)
W-O_3(×1)	2.249(6)
W-O Av.	1.951
Tm-O_4(×2)	2.184(6)
Tm-O_2(×2)	2.224(6)
Tm-O_1(×2)	2.342(6)
Tm-O Av.	2.25

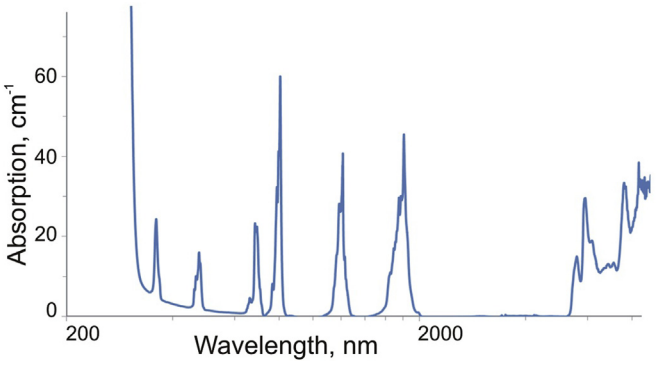

Fig. 5. Absorption spectrum of $LiTm(WO_4)_2$.

The refined structure corresponds to the $LiYb(WO_4)_2$ structural type. This structural type is closely related to wolframite and is based on a zigzag chain of edge-shared octahedra. The chains of the first type are built from WO_6 octahedra, whereas those of the second type, from alternating LiO_6 and TmO_6 octahedra; each type of chains occupies a separate layer perpendicular to the *c* axis (Fig. 1c).

The absorption spectrum of LTW crystal plate is presented in Fig. 5. The short-wavelength absorption edge is positioned at ~300 nm, while in the range of 350–2000 nm there are six absorption bands corresponded with transitions of Tm^{3+} ion from ground $^3H_6$ state to $^1D_2$, $^1G_4$, $^3F_3$, $^3H_4$, $^3H_5$, and $^3F_4$. Both the structure and intensity of the bands may vary depending on the thulium embedded matrix [30–33]. A wavelength range after 5 μm consists of vibrational absorption from the ground $^3H_6$ state.

Depending on the excitation wavelength, the crystal shows specific fluorescence of Tm^{3+} with the most intensive lines at ~450 nm ($^1D_2 \rightarrow {}^3F_4$) and ~800 nm ($^3H_4 \rightarrow {}^3H_6$) [28] (Fig. 6a and b). A

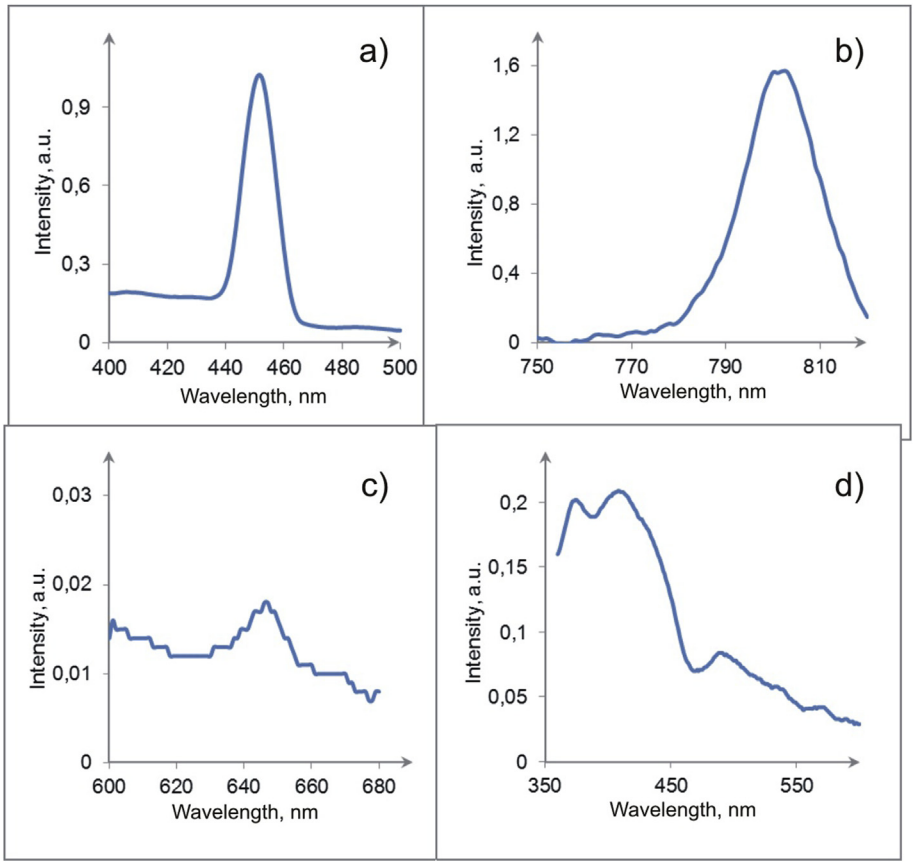

Fig. 6. Fluorescence spectra of $LiTm(WO_4)_2$.

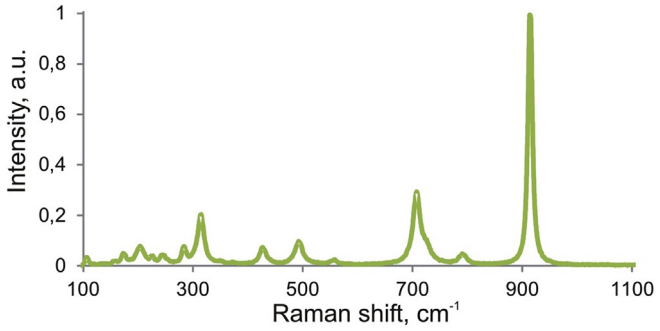

Fig. 7. Raman spectrum of $LiTm(WO_4)_2$.

weak transition $^1G_4 \rightarrow {}^3F_4$ [34] was observed at ~645 nm (Fig. 6c). Excitation to $^1D_2$ state induces fluorescence of the three above mentioned transitions, while the $^1G_4 \rightarrow {}^3F_4$ and $^3H_4 \rightarrow {}^3H_6$ transitions are observed for excitation to $^1G_4$ state. These states likely interact through relaxation processes. One of the specific thulium fluorescence line ($^3F_4 \rightarrow {}^3H_6$ transition) in the range of 1.6–2.1 μm [30] is not shown. Apart from the Tm fluorescence, the excitation to total absorption band (below 300 nm) results in low intensity emission in the 360–460 nm range (Fig. 6d), which is likely to be a defect related luminescence.

The use of excitation source at 785 nm coincides with the absorption band of $^3H_4$ state, so that intensive emission at 810 nm (Fig. 6b) instead of Raman spectrum was obtained. The 532 nm radiation source was used to record the Raman spectrum shown in Fig. 7. According to Ref. [35], major intensities in the spectra are likely due the chains of distorted WO_6 octahedra. Raman bands between 490 and 710 cm^{-1} are likely to result from W_2O_2 bridge system vibrations. Stretching and bending modes of WO_6 are located at higher and lower frequencies, respectively.

4. Conclusions

In this work a novel crystal of $LiTm(WO_4)_2$ was synthesized using solid state reaction and characterized using optical methods for the first time. Tm ions demonstrated classical electron transitions and, thus, the materials could be further studied in the scope of laser and luminescence applications. The compound is likely to melt congruently, however Czochralski growth method cannot be applied due to a phase transition. Flux growth could be adopted for epitaxial growth of active layers for micro-laser applications.

Acknowledgements

The research was supported by RSF grant #19-42-02003 in the part of crystal synthesis, project GF MES RK IRN AP05130794 and state assignment of IGM SB RAS.

References

[1] G.M. Greetham, P.M. Donaldson, C. Nation, I.V. Sazanovich, I.P. Clark, D.J. Shaw, A.W. Parker, M. Towrie, A 100 kHz time-resolved multiple-probe femtosecond to second infrared absorption spectrometer, Appl. Spectrosc. 70 (2016) 645–653.
[2] R. Akbari, K.A. Fedorova, E.U. Rafailov, A. Major, Diode-pumped ultrafast Yb:KGW laser with 56 fs pulses and multi-100 kW peak power based on SESAM and Kerr-lens mode locking, Appl. Phys. B 123 (2017) 123–126.
[3] P. Lecoq, Development of new scintillators for medical applications, Nucl. Instrum. Methods Phys. Res., Sect. A 809 (2016) 130–139.
[4] M. Guzik, E. Tomaszewicz, S.M. Kaczmarek, J. Cybińska, H. Fuks, Spectroscopic investigations of $Cd_{0.25}Gd_{0.50}\square_{0.25}WO_4:Eu^{3+}$ - a new promising red phosphor, J. Non-Cryst. Sol. 356 (2010) 1902–1907.
[5] L.J. Zhou, W.X. Wang, S.C. Yu, B. Nan, Y.G. Zhu, Y. Shi, H.H. Shi, X.Z. Zhao, Z.G. Lu, Single-phase $LiY(MoO_4)_{(2-x)}(WO_4)_{(x)}:Dy^{3+}, Eu^{3+}$ phosphors with white luminescence for white LEDs, Mater. Res. Bull. 84 (2016) 429–436.
[6] G.H. Kim, U. Kang, D. Heo, V.E. Yashin, A.V. Kulik, S.A. Chizhov, A compact femtosecond generator based on an Yb:KYW crystal with direct laser-diode pumping, J. Opt. Technol. 77 (2010) 225–229.
[7] P. Loiko, X. Mateos, S.Y. Choi, F. Rotermund, J.M. Serres, M. Aguilo, F. Diaz, K. Yumashev, U. Griebner, V. Petrov, Vibronic thulium laser at 2131 nm Q-switched by single-walled carbon nanotubes, J. Opt. Soc. Am. B 33 (2016) D19–D27.
[8] J.H. Liu, V. Petrov, H.J. Zhang, J.Y. Wang, M.H. Jiang, Efficient passively Q-switched laser operation of Yb in the disordered $NdGd(WO_4)_2$ crystal host, Opt. Lett. 32 (2007) 1728–1730.
[9] G.M. Kuz'micheva, D.A. Lis, K.A. Subbotin, V.B. Rybakov, E.V. Zharikov, Growth and structural X-ray investigations of scheelite-like single crystals Er, Ce:$NaLa(MoO_4)_2$ and Yb:$NaGd(WO_4)_2$, J. Cryst. Growth 275 (2005) 1835–1842.
[10] P.V. Klevtsov, R.F. Klevtsova, Polymorphism of the double molybdates and tungstates of mono- and trivalent metals with $M^+R^{3+}(EO_4)_2$, J. Struct. Chem. 18 (1977) 339–355.
[11] J.M. Postema, W.T. Fu, D.J.W. IJdo, Crystal structure of $LiLnW_2O_8$ (Ln= lanthanides and Y): an X-ray powder diffraction study, J. Solid State Chem. 184 (2011) 2004–2008.
[12] A.P.d.A. Marques, R. Künzel, N.K. Umisedo, R.M. Latini, E.M. Yoshimura, E. Okuno, Tm^{3+} doped barium molybdate: a potential long-lasting blue phosphor, J. Alloys Compd. 735 (2017) 707–717.
[13] I.M. Pinatti, P.F.S. Pereira, M. de Assis, E. Longo, I.L.V. Rosa, Rare earth doped silver tungstate for photoluminescent applications, J. Alloys Compd. 771 (2019) 433–447.
[14] X. Ren, M. Pei, C. Ming, A. Zhou, D. Ju, F. Song, Stable temperature characteristic of phosphate glass ceramic for white light-emitting diode, Micro & Nano Lett. 14 (2019) 113–115.
[15] P. Loiko, Y. Wang, J.M. Serres, X. Mateos, M. Aguiló, F. Díaz, L. Zhang, Z. Lin, H. Lin, G. Zhang, E. Vilejshikova, E. Dunina, A. Kornienko, L. Fomicheva, V. Petrov, U. Griebner, W. Chen, Monoclinic Tm:$MgWO_4$ crystal: crystal-field analysis, tunable and vibronic laser demonstration, J. Alloys Compd. 763 (2018) 581–591.
[16] E. Kifle, X. Mateos, P. Loiko, K. Yumashev, A. Yasukevich, V. Petrov, U. Griebner, M. Aguiló, F. Díaz, Graphene Q-switched Tm:$KY(WO_4)_2$ waveguide laser, Laser Phys. 27 (2017), 045801.
[17] M. Derbal, D. Ouadjaout, F. Siserir, V. Jubera, J.P. Chaminade, A. Garcia, O. Viraphong, M. Kadi Hannifi, Emission spectrum and simulated laser parameters of Yb^{3+}:$LiLu(WO_4)_2$ crystal, Opt. Mater. 32 (2010) 756–758.
[18] X. Huang, Z. Lin, Zushu Hu, L. Zhang, J. Huang, G. Wang, Growth, structure and spectroscopic characterizations of Nd^{3+}-doped $LiLa(WO_4)_2$ crystal, J. Cryst. Growth 269 (2004) 401–407.
[19] X. Huang, Z. Lin, L. Zhang, J. Chen, G. Wang, Growth, structure, and spectral characterization of $LiNd(WO_4)_2$, Cryst. Growth Des. 6 (2006) 2271–2274.
[20] X. Huang, G. Wang, Growth and optical characteristics of Yb^{3+}:β-$LiY(WO_4)_2$ crystal, Opt. Mater. 31 (2009) 919–922.
[21] D. Zhao, J.C. Shi, C.K. Nie, R.J. Zhang, Crystal structure and luminescent properties of two lithium lanthanide tungstate $LiLn(WO_4)_2$ (Ln = Sm, Eu), Optik 138 (2017) 476–486.
[22] V.K. Trunov, A.A. Evdokimov, Double tungstates of lithium and rare earth elements, Crystallography 19 (1975) 616–617.
[23] V.I. Spitsyn, V.K. Trunov, New data on double tungstates and molybdates of the $MeLn(EO_4)_2$ composition, Dokl. Akad. Nauk SSSR 185 (1969) 854–856.
[24] A. Rothkirch, G.D. Gatta, M. Meyer, S. Merkel, M. Merlini, H.P. Liermann, Single-crystal diffraction at the Extreme Conditions beamline P02.2: procedure for collecting and analyzing high-pressure single-crystal data, J. Synchrotron Radiat. 20 (2013) 711–720.
[25] G.M. Sheldrick, A short history of SHELX, Acta Crystallogr. Sect. A 64 (2008) 112–122.
[26] L.J. Farrugia, WinGX suite for small-molecule single-crystal crystallography, J. Appl. Crystallogr. 32 (1999) 837–838.
[27] B.H. Toby, R.B. Von Dreele, GSAS-II: the genesis of a modern open-source all purpose crystallography software package, J. Appl. Crystallogr. 46 (2013) 544–549.
[28] P.V. Klevtsov, C.P. Kozeeva, R.F. Klevtsova, N.A. Novgorodtseva, Preparation and properties of crystals of the $LiLn(WO_4)_2$ double tungstates for Ln = rare earth, Y, or Fe, Growth Cryst. 9 (1969) 107–109.
[29] N.G. Kononova, A.E. Kokh, RU Patent No. 2.195.520. Bul. No. vol. 36, 27.12.2002.
[30] Y. Lu, Y. Dai, J. Wang, Y. Yang, A. Dong, S. Li, B. Sun, Spectra and intensity parameters of Tm^{3+} ion in $YAlO_3$ crystal, Optic Commun. 273 (2007) 182–186.
[31] K.D. Knoll, Absorption and fluorescence spectra of Tm^{3+} in YVO and YPO, Phys. Status Solidi (b) 46 (1971) 553–559.
[32] J. Chrysochoos, A.H. Qusti, Intense blue luminescence spectra and lifetimes of Tm^{3+} in $POCl_3$:$SnCl_4$, J. Less Comm. Metal. 126 (1986) 161–167.
[33] V.I. Zhekov, G.G. Asatiani, Z.G. Melikishvili, G.A. Tsintsadze, T.I. Sanadze, T.D. Medoidze, G.I. Petriashvili, A.G. Papashvili, Absorption spectra and selective excitation of $Y_3Al_5O_{12}$: Tm^{3+} and $YLiF_4$: Tm^{3+} laser systems, Laser Phys. 10 (2000) 532–539.
[34] W. Ryba-Romanowski, S. Golab, I. Sokolska, G. Dominiak-Dzik, J. Zawadzka, M. Berkowski, J. Fink-Finowicki, M. Baba, Spectroscopic characterization of a Tm^{3+}:$SrGdGa_3O_7$ crystal, Appl. Phys. B 68 (1999) 199–205.
[35] J. Hanuza, M. Maczka, J. H van der Maas, Vibrational properties of double tungstates of the $M^IM^{III}(WO_4)_2$ family (M^I=Li, Na, K; M^{III}=Bi, Cr), J. Solid State Chem. 117 (1995) 177–188.